Trafficking dynamics of VEGFR1, VEGFR2, and NRP1 in human endothelial cells

Sarvenaz Sarabipour[1], Karina Kinghorn[2], Kaitlyn M Quigley[2], Anita Kovacs-Kasa[3], Brian H Annex[3], Victoria L Bautch[2,4], Feilim Mac Gabhann[1]

[1]Institute for Computational Medicine and Department of Biomedical Engineering, Johns Hopkins University, Baltimore, Maryland, United States

[2]Department of Biology, University of North Carolina, Chapel Hill, North Carolina, United States

[3]Vascular Biology Center and Department of Medicine, Medical College of Georgia at Augusta University

[4]McAllister Heart Institute, University of North Carolina, Chapel Hill, North Carolina, United States

Abstract

The vascular endothelial growth factor (VEGF) family of cytokines are key drivers of blood vessel growth and remodeling. These ligands act via multiple VEGF receptors (VEGFR) and co-receptors such as Neuropilin (NRP) expressed on endothelial cells. These membrane-associated receptors are not solely expressed on the cell surface, they move between the surface and intracellular locations, where they can function differently. The location of the receptor alters its ability to 'see' (access and bind to) its ligands, which regulates receptor activation; location also alters receptor exposure to subcellularly localized phosphatases, which regulates its deactivation. Thus, receptors in different subcellular locations initiate different signaling, both in terms of quantity and quality. Similarly, the local levels of co-expression of other receptors alters competition for ligands. Subcellular localization is controlled by intracellular trafficking processes, which thus control VEGFR activity; therefore, to understand VEGFR activity, we must understand receptor trafficking. Here, for the first time, we simultaneously quantify the trafficking of VEGFR1, VEGFR2, and NRP1 on the same cells - specifically human umbilical vein endothelial cells (HUVECs). We build a computational model describing the expression, interaction, and trafficking of these receptors, and use it to simulate cell culture experiments. We use new quantitative experimental data to parameterize the model, which then provides mechanistic insight into the trafficking and localization of this receptor network. We show that VEGFR2 and NRP1 trafficking is not the same on HUVECs as on non-human ECs; and we show that VEGFR1 trafficking is not the same as VEGFR2 trafficking, but rather is faster and weighted to intracellular expression, due to faster internalization and lower recycling, resulting in increased overall degradation. As a consequence, the VEGF receptors are not evenly distributed between the cell surface and intracellular locations, with a very low percentage of VEGFR1 being on the cell surface. Our findings have implications both for the sensing of extracellular ligands and for the composition of signaling complexes at the cell surface versus inside the cell.

Introduction

Vascular endothelial cells that line blood vessels undergo sprouting angiogenesis, an essential process for tissue maintenance and remodeling. While successes have been achieved in the inhibition of angiogenesis in cancer and retinopathy, over a dozen human clinical trials of VEGF delivery in patients with peripheral artery disease (PAD) and coronary artery disease (CAD) who suffer from vascular insufficiencies have failed to produce clinical gain [1–3]. Thus, there is a need to increase blood flow via promotion of functional collateral vascularization. The inability to successfully bridge treatment from animals to humans demonstrates that our understanding of the complexities of how the VEGF receptor system controls angiogenesis is far from complete.

Vascular endothelial growth factor receptors (VEGFRs) are members of the receptor tyrosine kinase (RTK) superfamily and key targets for pro- and anti-angiogenic therapies [4]. The receptors bind to ligands to mediate signaling that controls endothelial cell behaviors during angiogenesis [4,7]; ligand binding induces a structural change in the receptor that increases phosphorylation [5]. The receptors can also interact in the absence of ligands [5,6]. VEGFR1 and VEGFR2 both bind common isoforms of VEGF-A; VEGFR1 also binds to isoforms of placental growth factor (PlGF) and VEGF-B [8]. In the body, different tissues (and tissues in different states) express different levels of VEGF/PlGF family isoforms, and the outcome of VEGFR signaling results from the competition of ligands for the receptors and the competition of receptors for the ligands. Select isoforms of VEGF and PlGF also interact with co-receptors expressed on endothelial cells, including heparan sulfate proteoglycans (HSPGs) and Neuropilin-1 (NRP1); these isoform-selective co-receptors play an important role in how the cell ‘sees’ and interprets the extracellular cytokine milieu. There are also direct (receptor-receptor) and indirect (receptor-ligand-receptor) associations between NRP1, a transmembrane glycoprotein, and the VEGFRs.

Of particular note among the VEGFRs, VEGFR2 has been more extensively studied, while VEGFR1, despite being a key regulator of vascular development [7,9], has been less well understood [4,8]. VEGFR1 is alternatively spliced into a membrane-integral form (mVEGFR1 or

73 mFlt1), which we focus on here, and a soluble form (sVEGFR1 or sFlt) [10]. sVEGFR1 is not cell-
74 associated and lacks a kinase domain, rendering it unable to initiate intracellular signaling; it binds
75 VEGFs and PlGFs and thus regulates the amounts of these ligands available to membrane-
76 associated VEGFRs. In some situations, membrane-associated VEGFR1 (mFlt1) appears to
77 behave as a localized decoy receptor, titrating VEGF access to VEGFR2 via non-signaling
78 complex formation; for example, mVEGFR1 is involved in connection-site selection as vessels
79 anastomose [13]. However, there is also evidence that VEGFR1 induces signaling pathways in
80 its own right, on endothelial cells [11] or other cell types [12]. For example, VEGFR1 can signal
81 through a non-canonical STAT3 pathway (specifically, phosphorylation of STAT3 independent of
82 JAK-STAT) to promote angiogenesis and perfusion recovery in mice and humans; this is typically
83 blocked by an alternately spliced VEGF isoform, VEGFA-165b, and suppression of VEGFA-165b
84 allows VEGF-A165a to bind VEGFR1, VEGFR1's cytoplasmic tyrosine Y1333 to be
85 phosphorylated, and STAT3 to be activated. [11]. In addition, recent experiments using
86 endothelium-specific VEGFR deletions in mice showed that VEGFR1 deletion impacts vascular
87 density even on a VEGFR2-deleted background, suggesting that VEGFR1 functions by signaling
88 in its own right, not only as a decoy for VEGFR2 [14]. The stability and trafficking of VEGFR1
89 alters its local availability (receptor density) and can therefore affect VEGFR1's decoy and
90 signaling functions.

91 While the trafficking pathways of VEGFR2 are well defined, much less is understood or
92 quantified about the trafficking of VEGFRs and NRP1. And yet, trafficking of these receptors is
93 responsible for multiple points of control in the VEGF pathway. Trafficking controls the quantity of
94 receptors available on the cell surface to bind to extracellular ligands in the first place; it controls
95 the stability and turnover of these receptors, and the balance between internal and external
96 expression. Trafficking also controls the movement of receptors post-ligation and activation [15].
97 As we have shown previously for VEGFR2, this trafficking exposes receptors to different
98 phosphatases, which selectively deactivate specific tyrosines and therefore specific downstream

99 pathways [16]. When receptors are internalized, they have two possible fates: degradation or
100 recycling back to the surface. VEGFR2 and NRP1 are recycled via a Rab4a-dependent route
101 (sometimes referred to as ‘fast recycling’) or a Rab11a-dependent route (‘slow recycling') [2–4].
102 These two Rab-GTPases also control blood vessel formation and animal viability [17,18]. Both
103 unliganded and activated VEGFR2 are recycled [19,20]; however, how VEGFR1 internalization
104 is balanced with recycling and degradation has not previously been studied. NRP1 is also
105 trafficked and can impact VEGFR2 trafficking [16], but it is unclear how NRP1 affects VEGFR1
106 trafficking.

107 The VEGF-VEGFR system is targeted in many diseases, including ischemic diseases
108 such as peripheral artery disease, in an effort to modulate the vascular density and alter the extent
109 of perfusion of tissues. To design more effective therapies that target this system, a
110 comprehensive mechanistic understanding of how the VEGF-VEGFR system works is required.
111 Clearly, receptor trafficking plays an important role in this but has not yet been quantitatively
112 elucidated. For VEGFR2 and NRP1, trafficking has been studied *in vitro* [21–23] and *in silico*
113 [16,24,25], however previous computational models were based on measurements of receptors
114 in non-human cells, and/or in cells generated using overexpression of receptors or of trafficking
115 components. Thus, these previous models did not have detailed experimental measurements of
116 endogenous VEGFR1, VEGFR2, and NRP1 localization in human endothelial cells. Here, we
117 present such measurements and modeling for the first time; indeed, VEGFR1 trafficking is
118 investigated here for the first time in any cell type. To our knowledge, this is the first set of
119 VEGFR1, VEGFR2, and NRP1 trafficking experiments on the same human cell type, and the first
120 computational model to include detailed trafficking of VEGFR1, VEGFR2, and NRP1 explicitly.

121

122 ## Materials and Methods

123 ### Computational Model Construction

124 We developed a molecularly-detailed mechanistic computational model of membrane-integral
125 VEGF receptors, VEGFR1, VEGFR2, and Neuropilin-1, trafficking in human endothelial cells, and
126 parameterized it using experimental data from human endothelial cell culture. The model uses
127 coupled, nonlinear, deterministic ordinary differential equations to describe key biophysical and
128 biochemical reactions of receptor-receptor dimerization, and trafficking processes for receptors
129 (Figure 1). Binding and coupling reactions occur in every model compartment where associated
130 species are present. The model uses experimentally-derived surface receptor expression levels
131 and interaction kinetics for receptors expressed in HUVECs that have been previously measured
132 or derived (Supplementary Tables S1–S2) and incorporates geometry and initial concentrations
133 specific to the *in vitro* HUVEC cell culture experiments being simulated, including those previously
134 published and new experiments described here.

135 **Receptor binding reactions and trafficking processes.** In the model, we assume that VEGFR1
136 receptor monomers can undergo reversible homodimerization in the absence of ligands, as has
137 been shown for VEGFR2 [5,6]. The binding affinities and on- and off-rates of binding used here
138 are based on previously estimated reaction parameters (Supplementary Table S2). The model
139 includes five compartments: one extracellular (the fluid space outside the cell, i.e. culture media)
140 and four subcellular: cell surface; early endosomes (Rab4a-expressing and Rab5a-expressing
141 endosomes); recycling endosomes (Rab11a-expressing); and a degradation compartment
142 (representing lysosomes). Concentrations of components in each compartment are assumed to
143 be uniform (well mixed) but not constant. The model includes constant synthesis by the cell of
144 new VEGFR1, VEGFR2, and NRP1; the synthesis process inserts them into the cell surface
145 compartment. From there, movement of receptors between compartments occurs through first-
146 order transport processes; the trafficking processes are summarized in Figure 1. Surface
147 receptors are internalized to the early endosome compartment. From these endosomes,
148 receptors can either be degraded (via trafficking to lysosomes), recycled to the surface directly,

149 or trafficked to the Rab11a compartment for recycling; two recycling pathways are included
150 because previous evidence supports a role for both Rab4a and Rab11a endosomal recycling
151 pathways for VEGFR2 and NRP1 in endothelial cells [22]. The complete set of biochemical and
152 trafficking reactions can be found in the Supplementary tables S1-S4. The balance of synthesis,
153 degradation, and trafficking results in a steady-state, constant surface level of VEGFR1, VEGFR2,
154 and NRP1 populations in the absence of ligand. As part of the parameter optimization process,
155 this initial surface level of VEGFR1, VEGFR2, and NRP1 matches published experimental data
156 [26].

157 **Model solution and outputs.** The complete model contains 314 molecular species, including
158 separately tracking the levels of each receptor or receptor complex at each subcellular location
159 (plasma membrane, Rab4a/5a endosomes, Rab11a endosomes, lysosome). Code to simulate
160 the set of coupled ordinary differential equations that comprise this model were generated using
161 the rule-based BioNetGen software [27] and numerically solved using MATLAB. The model
162 outputs are the concentrations of each molecule or molecular complex over time. To facilitate
163 direct comparison to experimental data, the output concentrations of specific molecules or
164 complexes are combined into aggregated quantities of interest; for example, the total VEGFR1
165 levels on the cell surface is the sum of VEGFR1 present in multiple different complexes.
166 Depending on the experimental measurement, e.g. levels of proteins from whole cell lysates, or
167 only surface proteins isolated via biotin labeling, the appropriate molecular complexes from the
168 appropriate subcellular compartments in the model are aggregated to better compare the
169 simulated results to the experimental results.

170 **Model parameter optimization.** For HUVECs, we estimated the values of 15 receptor trafficking
171 parameters and 3 receptor production rate parameters in the absence of exogenous ligands.
172 These parameter estimates are based on optimization (fitting) to the results of new receptor
173 expression measurements and surface/internal expression percentages, described below,

174 including perturbations to receptor trafficking, that provide the most detailed and complete
175 quantitative data yet on VEGFR1, VEGFR2, and NRP1 trafficking from a single consistent set of
176 human endothelial cell experiments. Previously-published measurements of endogenous cell
177 surface VEGFR1, VEGFR2, and NRP1 (1,800, 4,900, and 68,000 receptors per cell respectively
178 for HUVECs) were also part of the optimization data [26]. When comparing simulation results to
179 experimental results, the simulation initial conditions, geometry, and parameter perturbations are
180 faithful to the experimental protocol for that experiment; and the experimental measurements
181 (such as surface and whole-cell receptor expression) are directly compared to the relevant
182 aggregated model outputs. As the experimental data are primarily western blots, we compare
183 normalized values of the experimental results to normalized values of the simulation results. For
184 optimization, we used a nonlinear least-squares optimization approach with the Levenberg-
185 Marquardt algorithm in MATLAB. As is common for biological systems with many components
186 and measurements, the experimental results available do not uniquely determine a single best fit
187 parameter set. Therefore, we initiated many separate optimization runs with different randomly
188 generated initial values, and bounded the parameters with a large range (five orders of magnitude:
189 $[10^{-6}, 10^{-1}]$ s^{-1}). Some parameters exhibit more uncertainty than others, but all parameters were
190 constrained to some degree (Figure 4).
191 **Sensitivity Analysis.** We performed univariate local sensitivity analysis to identify parameters
192 that most strongly affect model outputs. Key parameters were varied and the change in each
193 selected output calculated. We calculate the relative sensitivity metric as % change in output
194 divided by % change in parameter. Model outputs selected included levels of expression of the
195 receptor in the whole-cell and in subcellular locations (Figure 6).
196
197 **Experimental Methods**
198 **Cell culture.** Human umbilical vein endothelial cells (HUVEC) (see Supplementary Table S5 for
199 manufacturers, catalog numbers, and other details of all reagents used) were cultured at 37 °C in

200 EBM-2 medium supplemented with a bullet kit (EGM-2) and used at passages 3–5. For each
201 experiment, cells were used when they became confluent (2-3 days post-plating).
202
203 **Perturbations.** Several treatments were used to inhibit specific processes in the receptor
204 trafficking system (Figure 1). To inhibit new protein synthesis, following serum starvation HUVEC
205 were treated with 50 µg/mL cycloheximide (CHX). To inhibit lysosomal degradation, serum-
206 starved (overnight) HUVEC were treated with 10 $\mu g.mL^{-1}$ of chloroquine (CHQ). To deplete
207 expression of recycling-associated proteins Rab4a and Rab11a in HUVEC, approximately $1x10^6$
208 cells were suspended in 100 ml nucleofector solution before adding 50–150 pmol of siRNA
209 (Silencer Select Locked Nucleic Acids) and using the A-034 program of the Amaxa Nucleofector
210 system for electroporation. Cells were transfected with control (non-targeting) siRNA duplex and
211 siRNA duplex targeting Rab4a and/or Rab11a. After 48 hr, the cells were serum-starved
212 (OptiMem + 0.1% FBS) for 18 hr, followed by CHX or CHQ addition.
213
214 **Whole cell protein isolation.** For selected experiments, total protein expression of VEGFR1,
215 VEGFR2, and NRP1 from whole cell lysates was measured. At appropriate time points, RIPA
216 buffer (50 mM Tris HCl, 150 mM NaCl, 1.0% (v/v) NP-40, 0.5% (w/v) Sodium Deoxycholate, 1.0
217 mM EDTA, 0.1% (w/v) SDS and 0.01% (w/v) sodium azide) and protease/phosphatase inhibitor
218 (Cell Signaling) at a pH of 7.4 was added to the plates, lysates were collected with cell scrapers,
219 subsequently boiled for 5 min at 95 °C, and used for immunoblot analysis as described below.
220 Experiments were repeated three times.
221
222 **Internal and cell surface protein isolation.** For other experiments, the protein expression of
223 receptors on the cell surface and expression inside the cell were separated and measured.
224 Biotinylation and isolation of cell surface proteins was performed according to the manufacturer's
225 protocol (Pierce™ Cell Surface Biotinylation and Protein Isolation Kit, cat#A44390). Briefly,

226 serum-starved HUVEC were washed twice in 6 ml of ice-cold PBS (Sigma-Aldrich) to stop
227 internalization. Surface VEGFR1, VEGFR2, and NRP1 were labeled with 0.25 $mg.ml^{-1}$ of the
228 membrane-impermeant biotinylation reagent EZ-link Sulfo-NHS-SS-Biotin (ThermoFisher
229 Scientific) at 4°C for 30 min with constant rocking. The unreacted biotinylation reagent was
230 quenched by incubation with 50 mM glycine. HUVEC were washed twice with ice-cold PBS and
231 removed from the plate by gently scraping. After centrifugation at 800g for 5 min at 4°C, cells
232 were lysed using the provided lysis buffer supplemented with protease/phosphatase inhibitors
233 (Cell Signaling Technologies). A percentage of the total lysate was reserved for total protein
234 analysis, and the rest was put over a NeutrAvidin Agarose slurry-containing spin column
235 (ThermoFisher) at 4°C for 1 hr. Flow-through was collected in a given volume (same for all
236 samples), and the column was then eluted with 1 M dithiothreitol (DTT), and the eluate was
237 resuspended in the same volume as the flow-through, to facilitate determination of
238 surface:internal ratios. Experiments were repeated three times.
239
240 **Immunoblots.** Immunoblots were performed as previously described [18]. Briefly, whole cell
241 lysates, or cell surface and internal fractions, were collected as described above. For whole cell
242 lysates, approximately 10µg of protein was separated by SDS-PAGE on 10% Tris-Acetate gels
243 and transferred onto PVDF membranes. For biotin labeling experiments, equal volumes of the
244 flow-through (~10µg) and eluate were loaded to facilitate determination of surface:internal ratios.
245 Membranes were blocked for 1 hr in OneBlock (Prometheus) and incubated at 4°C with primary
246 antibodies (Supplementary Table S5) in OneBlock overnight. Membranes were washed 3X in
247 PBST (PBS 0.1% Tween-20) before adding HRP-conjugated secondary antibodies for 1 hr at RT.
248 Secondary antibody was removed and membranes washed four times in PBST before addition of
249 Luminata Forte (Millipore). See Supplementary Table S5 for details of antibodies, inhibitors and
250 siRNAs used for this study. BioRad software was used to image the western blots, and ImageJ

251 software was used to isolate and quantify the specific bands produced by the antibody. Loading
252 control (typically alpha tubulin) was used to normalize amount of total protein present.
253

254 ## Results

255 **VEGF receptors exhibit different stability and turnover on HUVECs**

256 Under normoxic culture conditions, we measured the whole-cell expression levels of VEGFR1,
257 VEGFR2, and NRP1 proteins in serum-starved primary HUVEC in the absence of exogenous
258 ligands. We compared untreated cells to cells treated with 50 $ug.mL^{-1}$ cycloheximide (CHX) to
259 inhibit new protein synthesis and reveal the dynamics of trafficking and degradation not balanced
260 by new protein synthesis. Over time, NRP1 did not exhibit significant turnover, but rather was
261 stable throughout the experiment (Figure 2A). In contrast, whole-cell levels of VEGFR1 and
262 VEGFR2 decreased quickly, with half-lives of approximately 45 minutes for VEGFR1 and 75-90
263 minutes for VEGFR2; this was consistent with previous measurements of VEGFR2 loss following
264 CHX in other HUVEC studies [19]. Although VEGFR1 was suggested to be more stable than
265 VEGFR2 in the absence of ligand [18,29], here we carefully validated a different VEGFR1
266 antibody to ensure that it specifically identifies membrane-integral VEGFR1 (Supplementary
267 Figure S1).
268

269 **VEGF receptors exhibit different localization patterns (cell surface vs intracellular)**

270 Whole cell expression of receptors gives a partial view of receptor dynamics; to further refine
271 receptor localization we measured the cell-surface and intracellular distribution of VEGFR1,
272 VEGFR2, and NRP1 via biotin labeling of cell surface proteins on serum-starved HUVECs. Absent
273 additional perturbation, the percentage of each receptor expressed on the surface estimated from
274 these results (Figure 2B) is 10%, 51%, and 74% for VEGFR1, VEGFR2, and NRP1, respectively.
275 This is consistent with previous estimates of ~55-60% for VEGFR2 surface localization [30]; in

276 most endothelial cell types, NRP1 is present at cell surface densities higher than those of
277 VEGFR2 [26], and here we show that this difference is likely partly due to NRP1 being biased
278 towards surface expression. A previous estimate of ~25% VEGFR1 on the surface may have
279 been a result of overcounting using an antibody that is not specific for membrane-integral
280 VEGFR1 [29]. The absolute levels of VEGFR1 on the cell surface have been measured previously
281 [26] as being slightly lower or slightly higher than VEGFR2 levels, depending on cell type; however
282 the new observation that little of the total VEGFR1 is on the plasma membrane (with most of the
283 receptor being intracellular) has significant implications for how local receptor compositions differ.
284

285 **Recycling pathway perturbations**

286 Early endosomes sort internalized cargo for recycling or degradation, and proteins typically
287 recycle from endosomes to the cell surface in a Rab4a-dependent or Rab11a-dependent manner.
288 We disrupted these recycling pathways via siRNA-mediated knockdown of Rab4a and Rab11a in
289 HUVEC. Whole cell expression of VEGFR1, VEGFR2, and NRP1 was measured following siRNA-
290 Rab4a, siRNA-Rab11a, or siRNA-Rab4a/siRNA-Rab11a treatment; this was done in the absence
291 and presence of 50 $ug.mL^{-1}$ CHX to assess changes to stability/turnover. The levels of VEGFR1,
292 VEGFR2, and NRP1 were essentially unaffected by Rab4a knockdown and Rab11a knockdown
293 experiments, and receptor stability in response to CHX was similarly unaffected (Figure 2C-D).
294

295 **Previous estimates of receptor trafficking do not match HUVEC data**

296 The goal of generating a computational model of VEGF receptor trafficking was to understand
297 and quantify the mechanistic basis for the observed experimental data. We previously estimated
298 trafficking parameters for VEGFR2 and NRP1 [16,25], however those parameters were based on
299 data from porcine aortic endothelial cells (PAECs) into which human receptors were transfected
300 and overexpressed [22]. We also previously used those PAEC-derived parameters to simulate
301 endothelial cells in human *in vivo* models [25]. To check whether those parameters are consistent

302 with the new HUVEC data, we used them in our trafficking model and simulated the HUVEC
303 experiments described above. The simulated surface vs internal levels of VEGFR2 and NRP1
304 appear to match well - perhaps these are similar on PAECs and HUVEC. However, using similar
305 trafficking parameters for VEGFR1 and VEGFR2 (this assumption was used in previous models
306 [25]) was inaccurate in HUVEC, since the simulated surface levels of VEGFR1 with that
307 assumption were higher than measured here. In addition, the stability of VEGFR1 and VEGFR2
308 in the simulations following CHX-induced protein synthesis shutdown was higher than measured.
309 These discrepancies suggest that the trafficking model parameters from the PAEC study are not
310 applicable to HUVEC (Figure 3A-B). This might be due to the species difference, tissue of origin
311 differences, or to differences in levels of receptor expression.
312
313 **New estimates of VEGF receptor trafficking in HUVEC**
314 Since the previous estimates for trafficking parameters did not fit the HUVEC data well, we
315 performed a new optimization of all model trafficking parameters for VEGFR1, VEGFR2, and
316 NRP1, using the experimental data from HUVEC (Figure 2, 5A). We performed the optimization
317 over a hundred times, and found that while there is not a single unique solution to the 18-
318 parameter optimization, most of the parameters are well constrained (Figure 4), particularly
319 receptor production, internalization, and degradation. Bearing in mind that the parameter
320 distributions shown are the aggregation of individual optimization parameter sets, we took the
321 geometric mean of each to create an estimated parameter set to test against the observed data.
322 Simulations using these parameters show good reproduction of the HUVEC data (Figure 5A-C).
323 For example, the receptor stability/turnover dynamics following CHX are reproduced for all three
324 receptors (Figure 5F-I); the percentage of each receptor that is present on the surface is matched
325 (Figure 5F-I); and the response to Rab4a and Rab11a knockdowns is similarly consistent (Figure
326 5F-I). Exploration of the parameter estimates highlights the mechanistic differences across the
327 receptors: VEGFR1 has the highest internalization rate constant, while VEGFR2 and NRP1 have

328 similar values; NRP has the slowest degradation rate constant, while VEGFR1 and VEGFR2 are
329 similar; NRP1 also has the highest recycling rates, with VEGFR1 and VEGFR2 being close to
330 each other (VEGFR1 being perhaps slightly faster via the Rab11a pathway) (Figure 4). In addition,
331 the production rates of the three receptors are comparable, suggesting that the observed receptor
332 levels are primarily controlled by trafficking and degradation.
333
334 **Sensitivity analysis**
335 We performed local sensitivity analysis to identify which of the trafficking parameters most
336 strongly affect key model outputs. Model outputs observed here are the same outputs that we
337 compare to experimental data - whole cell receptor expression, surface expression, intracellular
338 expression, and the percentage of each receptor on the cell surface. Trafficking parameters were
339 increased by 5%, and the percent change in each output was calculated (Figure 6). Increased
340 production of VEGFR1 or VEGFR2 increased receptor levels evenly across the cell; however,
341 production of NRP1 followed a more nonlinear path, with increased NRP1 production rates
342 causing large (hyperlinear) increases in NRP1 levels. NRP1 levels are also highly dependent on
343 VEGFR1 but not VEGFR2 production; this is likely due to formation of VEGFR1-NRP1 complexes
344 [31]; these complexes have a faster internalization and degradation rate and therefore deplete
345 NRP1 overall. All receptors are sensitive to changes in the degradation rate constant, although
346 NRP1 is less sensitive, presumably because it is already very low and increased degradation also
347 leads to a slight bias towards surface expression. Internalization has a stronger effect on surface
348 receptor levels (decreasing them) than it does on the internal levels, which are controlled primarily
349 by the balance of production and degradation. As a result of VEGFR1 being primarily intracellular
350 while VEGFR2 is more equally distributed between the surface and intracellular locations,
351 increased internalization has a much larger effect on total VEGFR2 cell levels than those of
352 VEGFR1. Finally, the predominance of Rab4-pathway recycling for VEGFR2 can be seen in the

353 sensitivity analysis results, along with evidence that the pathways are redundant and neither
354 receptor uses one exclusively.
355
356 **Overall transport rates of VEGFR1, VEGFR2 and NRP1**
357 We calculated the net rate of receptor movement in surface and endosomal compartments (Figure
358 7) to examine the contributions of each trafficking process to the steady-state distribution. At
359 steady-state, the model predicts a concentration (receptor density) of VEGFR1, VEGFR2, and
360 NRP1 complexes in the plasma membrane and in each of the endosomal compartments (Figure
361 1). The parameters calculated for the model are rate constants, and the overall rate of transport
362 for each process is the rate constant multiplied by the relevant concentration. A rate constant
363 could be high, but if the corresponding concentration is low, then the rate of movement will be
364 low; note that VEGFR1, VEGFR2 and NRP1 are not uniformly distributed across cellular
365 compartments - for HUVEC, cell surface levels of these receptors used in our model and based
366 on experimental data [26] are 1,800 VEGFR1, 4,900 VEGFR2, and 68,000 NRP1 per cell. Inside
367 the cell, the balance is different: 16,200 VEGFR1, 4,010 VEGFR2, and 19,180 NRP1 per cell
368 (Figure 7A). At steady state, the transport rates in and out of each compartment (subcellular
369 location) are balanced, so that 'net' rates of receptor movement are close to zero. For the Rab11-
370 recycling pathway endosomes, the receptors coming in from Rab4a are balanced by receptors
371 leaving via recycling to the surface (Figure 7C). For Rab4 early endosomes, receptors due to
372 internalization from the surface are balanced by the sum of receptors being degraded or recycled
373 via both pathways. For the cell surface, receptors out due to internalization are balanced by the
374 sum of receptors in via new synthesis and two recycling pathways. The internalization rate of
375 VEGFR1 was found to be 4.0×10^{-2} s^{-1}, for a half-life (residence time on the surface) of $\ln(2)/k_{int}$
376 = 27 seconds. For VEGFR2, half-life (residence time on the surface) is 4.5 minutes, and NRP1,
377 6 minutes. These are short compared to the overall half-life of the receptors (Figure 2A), because
378 once internalized, most of the receptors are recycled rather than degraded, emphasizing the

379 dynamic nature of receptor trafficking and cycling between the surface and internal receptor pools
380 (even for the highly stable NRP1). Any perturbations - for example, addition of CHX, CHQ, or
381 depletion via siRNA - in addition to its effect on the appropriate rate constant, would result in
382 changes to the local receptor concentrations, changes to the related overall rates, and (at least
383 transiently) changes to the net rates of movement (which is what enables the local receptor
384 concentration changes).
385
386 We can directly compare rate constants for processes that act on the same set of receptors (for
387 example, the processes that lead from a certain subcellular location). This is most obvious when
388 looking at the early endosomes, which function as the main crossroads in the model (Figure 1,
389 Figure 7B marked 'Rab4a'). First, comparing the two major fates of endosomal receptors
390 (recycling and degradation), while the combined recycling rate constants via the two pathways is
391 greater than degradation rate for each of the three receptors, the ratios are very different: 19:1,
392 11:1 and over 7000:1 for VEGFR1, VEGFR2, and NRP1 respectively (Figure 7B, left). This means
393 that for every VEGFR1 degraded, 19 are recycled; or viewed another way, there is an
394 internalization-recycling loop for which a VEGFR1 makes on average 19 in-out loops before
395 internalization; VEGFR2 receptors undergo fewer and NRP1 very many more internalization-
396 recycling loops, showing that despite the stability (lifetime) of receptors on the cell overall (Figure
397 2A), there is also frequent movement between the surface and intracellular locations; the
398 receptors are more likely to be recycled than degraded while in the intracellular locations. Within
399 recycling, the receptors are biased differently between the Rab4a- and Rab11a-dependent
400 pathways (Figure 7B, middle). VEGFR2 preferentially uses Rab4a, while NRP1 and VEGFR1 use
401 the Rab4a and Rab11a pathways more equally; none of the receptors uses one pathway
402 exclusively, which is in keeping with previously observed VEGFR2 and NRP1 observations
403 [16,22] and with the redundancy shown by the knockdown experiments here. Using a similar
404 analysis, we can see the mechanistic basis for the differently-skewed surface vs internal levels of

405 the receptors (Figure 7B, right): the rate constant for internalization is significantly larger than that
406 of recycling for VEGFR1, but the inverse for NRP1. VEGFR2 is much more balanced, reflecting
407 the almost-even distribution of VEGFR2 between the surface and intracellular locations.
408
409 **Chloroquine (CHQ) and VEGFR1 degradation.** We previously showed that loss of new protein
410 synthesis resulted in a decrease in VEGFR1 levels over time as the receptor is degraded. The
411 consequence of inhibited degradation, if production is unchanged, should be an increase in
412 receptor levels. We treated cells with Chloroquine (CHQ), an inhibitor of lysosomal degradation,
413 and indeed see VEGFR1 accumulation (Figure 8). Using computational simulations that recreate
414 the conditions of the CHQ experiments, we estimate that this observed increase in VEGFR1 levels
415 is consistent with CHQ treatment inhibiting approximately 42% of VEGFR1 degradation; if
416 VEGFR1 degradation were completely inhibited, the predicted accumulation of VEGFR1 would
417 be even higher. This suggests that at least half of VEGFR1 loss is through non-lysosomal
418 degradation pathways, i.e. is not inhibited by CHQ; alternatively, the accumulation of VEGFR1
419 may cause a downregulation of VEGFR1 synthesis to compensate. VEGFR2 and NRP1 levels
420 did not increase, again suggesting non-lysosomal degradation pathways or adaptation of
421 production to prevent receptor build up.
422
423 **Discussion**
424 The intracellular trafficking of receptors is central to the sensing of ligands and the specificity of
425 downstream signaling. Trafficking that differs between receptors, or between cells, or becomes
426 altered within the same cell type based on condition, results in different surface and total receptor
427 levels, affecting availability to ligands, and exposure to different regulators, such as
428 phosphatases, that can result in different signaling. Specifically, for the VEGF system, with
429 multiple receptors (VEGFR1, VEGFR2, and NRP1) competing and cooperating, the local
430 expression of each of the receptors influences the ligand binding and activation of the others; they

431 form a system. The intracellular location of VEGFR2, in particular, influences the downstream
432 signaling pathways and cellular behaviors that are set in motion, and this impacts tissue-level
433 properties such as vascular network architecture and function [16]. In this study, we quantified
434 VEGF receptor trafficking rates and distribution in HUVEC using a mechanistic computational
435 model fitted to detailed new experimental data.

436 While there are some previous estimates of VEGF receptor trafficking, this is the first
437 quantitative rate analysis of VEGFR trafficking in human endothelial cells. It is of particular
438 importance that VEGFR1, VEGFR2, and NRP1 were measured in the same cell type and at the
439 same time, because of the interdependence of these receptors. We compared these new results
440 to VEGFR2 and NRP1 parameters obtained for a related computational model [16] using
441 experimental data from porcine aortic endothelial cells (PAECs) [22] and found that values were
442 not consistent between the studies. There are multiple reasons why VEGFR trafficking may be
443 different in the PAEC study versus this HUVEC study, including different species of the cells and
444 different tissue origins of the cells. Moreover, human VEGFR2 and NRP1 were overexpressed in
445 the PAECs, and the PAEC study also used data from overexpression of tagged Rab proteins,
446 which can impact Rab biogenesis and alter endosomal trafficking [33]. The rate constants of
447 HUVEC trafficking of VEGFRs quantified here are in general higher (faster) than those identified
448 from PAECs, with the exception of NRP1 degradation (Figure 3A, 5A). The fast kinetics of
449 endogenous proteins indicate a highly active system, with frequent movement between
450 intracellular compartments, indicative of cells ready to respond to extracellular stimulation.

451 Given the differences between previous trafficking parameters and the parameters
452 described here, it may be important in the future to quantify trafficking rates by species and cell
453 type, including across human endothelial cells of different tissue origin [26], or cells under different
454 pathological conditions such as hypoxia. For example, endothelial cells in different tissues
455 express different amounts of VEGF receptors [26,31,32]. In addition, not only does receptor

456 trafficking determine the availability of receptors locally to interact with ligands and with each
457 other, but also the binding of ligands and activation of receptors can influence trafficking.

458 A key observation from this study is that trafficking of the three VEGF receptors studied is
459 quite different. NRP1 is highly stable, with very low turnover as evidenced by consistent
460 expression after cessation of new protein synthesis. Although it is stable on the cell, the
461 mechanistic rate constants suggest that NRP1 is, like the other receptors, actively and rapidly
462 exchanged between the surface and endosomes. VEGFR1 and VEGFR2 are much less stable,
463 and their levels decline rapidly when new protein synthesis is blocked. This propensity for high
464 production and high degradation may be relevant to sensitivity to microenvironmental ligand
465 levels, and to downregulation of or adaptation to those stimuli. The trafficking of VEGFR1 and
466 VEGFR2 are also different, perhaps most obviously in the resulting differences in receptor levels
467 on the cell surface and internally. Most VEGFR1 appears to be intracellular, while VEGFR2 is
468 balanced between the two locations. In terms of absolute numbers of receptors, this means that
469 VEGFR2 is in excess on the cell surface, but VEGFR1 is in excess intracellularly. These different
470 subcellular regions (further distinguished by a bias towards surface expression for NRP1) are
471 therefore very different domains for ligand binding and downstream signaling, and the implications
472 of these local levels will need further study.

473 VEGFR1 was a particular focus of our study due to it being understudied compared to
474 VEGFR2. Quantifying VEGFR1 trafficking in the same experiments as VEGFR2 and NRP1 is
475 important, as these receptors are commonly co-expressed on endothelial cells and can interact.
476 VEGFR1 and NRP1, in particular, can interact directly in the absence of ligands (unlike VEGFR2
477 and NRP1) [32], and this VEGFR1-NRP1 complex forms an important part of the computational
478 model. A key assumption made here was that this complex trafficked at rates similar to VEGFR1;
479 identifying an independent set of rate constants for this complex was not possible while measuring
480 the receptors independently. We also tested an alternate assumption that the rates for VEGFR1-
481 NRP1 would be similar to those for NRP1, however this did not provide a good fit to the

experimental data. This VEGFR1-NRP1 complex has important consequences, including exhibiting ligand-binding specificity that impacts not just VEGFR1 binding but also ligand availability to VEGFR2. The presence of the complex also partly explains the low degradation rate constant of NRP1 in the model, in that the newly produced NRP1 in the simulations is not balanced at steady state by NRP1 degradation but rather by the combined degradation of NRP1 and VEGFR1-NRP1 , and this is mostly through degradation of the VEGFR1-NRP1 complex. When new protein synthesis is stopped, VEGFR1 decreases, VEGFR1-NRP1 levels decrease, and overall NRP1 protein levels remain stable as NRP1 alone is degraded slowly. Notably, when VEGFR1 or NRP1 production rates are increased (as in our sensitivity analysis, Figure 6), the effects on NRP1 levels are very strong, as the ratio of NRP1:VEGFR1-NRP1 changes and thus the aggregate degradation of NRP1 changes.

Combining comprehensive quantitative experimental data with mechanistic computational models has enabled us to identify which subcellular pathways are most influential for trafficking of each of the VEGF receptors, and to gain insight into how the VEGF receptor system is in quite a different state (different relative levels of the receptors) in different parts of the cell. This local regulation and the local conditions likely play an important role in response to ligand stimulation, and can potentially be harnessed to enhance therapeutic targeting of the VEGF system.

Author contributions

SS and FMG designed and wrote the code, performed data visualization, and wrote the original draft of the manuscript. KK, KMQ, and VLB planned and KK and KMQ performed the experiments and experimental data analysis. FMG, VLB, and BHA acquired resources and funding. SS, FMG, KMQ, KK, VLB, AKK, and BHA performed conceptualization, formal analysis, investigation, methodology, validation, and wrote, reviewed and edited the manuscript.

Conflicts of interest

The authors declare no conflict of interest.

Acknowledgements

This work was supported by NIH grant R01-GM129074.

Supplementary File

Contains five Tables and one Figure.

518 **FIGURES**
519

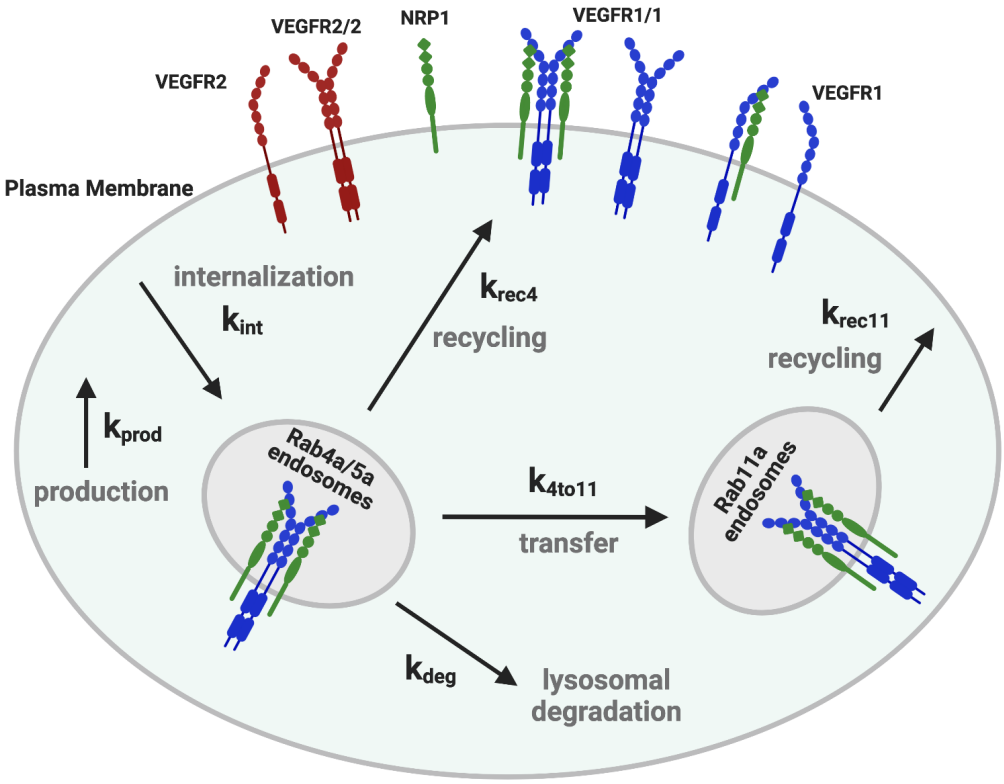

520
521
522
523 **Figure 1. Schematic of molecular interactions of the computational model.** Cellular
524 biophysical and biochemical reactions between VEGFR1, VEGFR2 and NRP1 receptors. The
525 receptors can homodimerize (at a lower level than that induced by ligands), and unlike VEGFR2,
526 VEGFR1 can form a complex with NRP1 in the absence of ligands [32]. During trafficking, surface
527 protein complexes (monomeric, dimeric, or higher order) can be internalized (rate constants
528 denoted k_{int}). Early endosomal ("Rab4a/5a") receptors can be degraded (rate constant k_{deg}),
529 recycled (rate constant k_{rec4}), or transferred to the Rab11a compartment (rate constant k_{4to11})
530 which leads to an additional recycling pathway (rate constant k_{rec11}). New surface receptors
531 (monomers) are produced at rate k_{prod}. Each of the rate constant values can be different for the
532 different receptors. Reaction rates and species concentrations are detailed in Supplementary
533 Tables S1-S4.
534
535

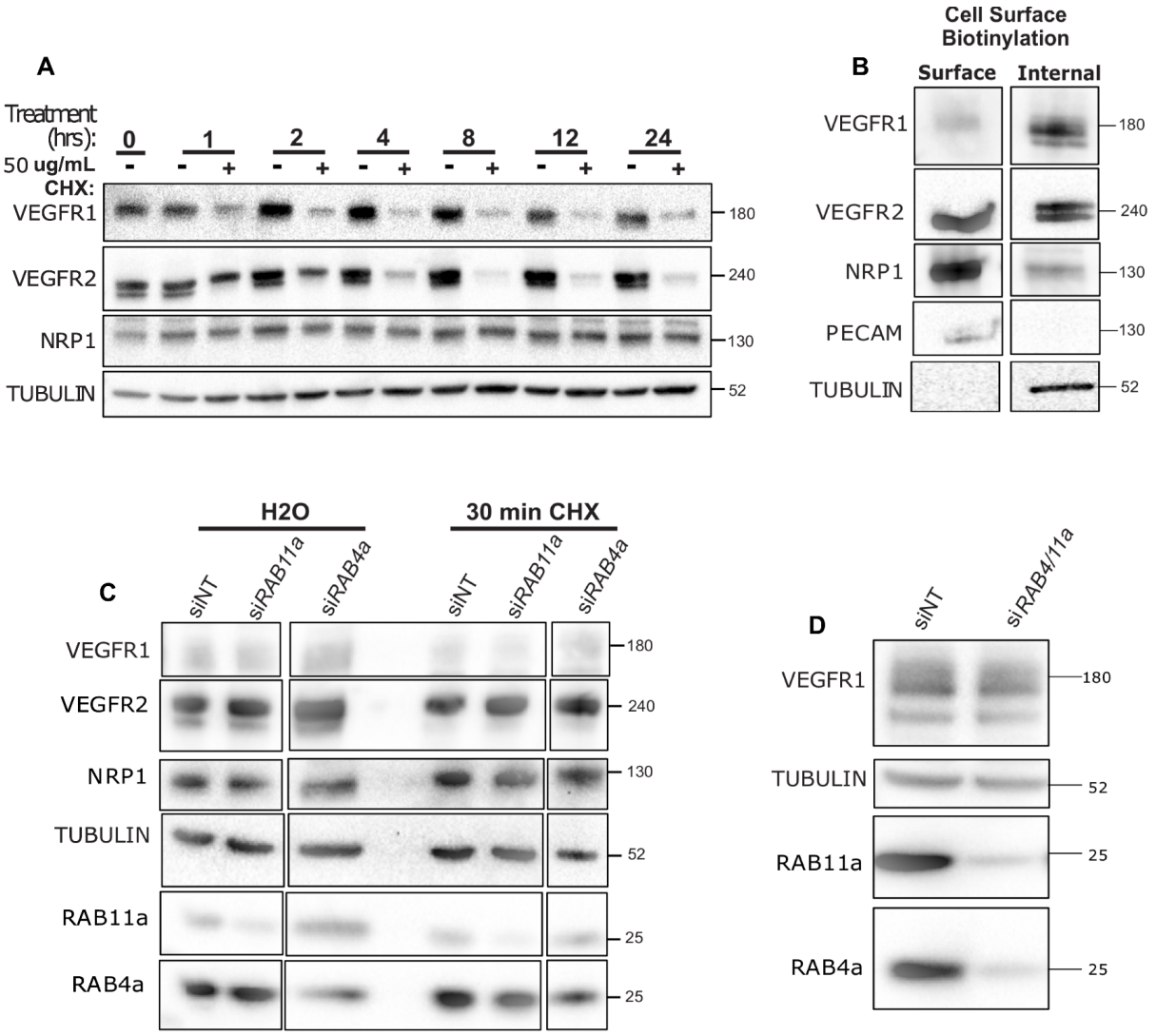

Figure 2. Experimental measures of VEGFR1, VEGFR2, and NRP1: whole-cell and surface levels in HUVEC. Western blot of total HUVEC lysates treated as indicated for 1-24 hours with 50 µg/ml cycloheximide (CHX) and stained for VEGFR1, VEGFR2 and NRP1. Representative of n=3 replicates. **B,** Western blot of biotin labeling assay to measure surface and internal VEGFR1, VEGFR2, and NRP1 levels in HUVEC. Representative of n=3 replicates. **C,** Western blot of VEGFR receptor levels following Rab4a or Rab11a siRNA treatment shows similar receptor stability as in response to CHX alone. Additional measurements at 60, 90, 120 and 240 min showed similar results (data not shown). Representative of n=3 replicates. **D,** Western blot showing the effect on VEGFR1 levels of depletion of both Rab4a and Rab11a.

A

Previously estimated parameters (2015-2017)				
Parameter	**Description**	**VEGFR1 (s^{-1})**	**VEGFR2 (s^{-1})**	**NRP1 (s^{-1})**
kint	Internalization	2.6×10^{-3}	2.6×10^{-3}	2.6×10^{-3}
kdeg	Degradation	8.6×10^{-6}	8.6×10^{-6}	3.8×10^{-4}
krec4	Early recycling	3.8×10^{-3}	3.8×10^{-3}	3.8×10^{-5}
k4to11	Pre-recycling	1.0×10^{-5}	1.0×10^{-5}	1.9×10^{-2}
krec11	Late recycling	1.4×10^{-4}	1.4×10^{-4}	1.4×10^{-2}
kprod	production rate	1.0×10^{-4}	2.8×10^{-4}	3.5×10^{-3}

B

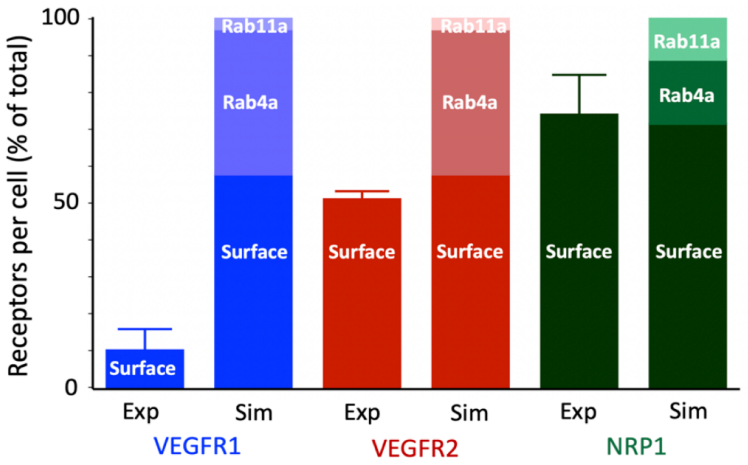

C

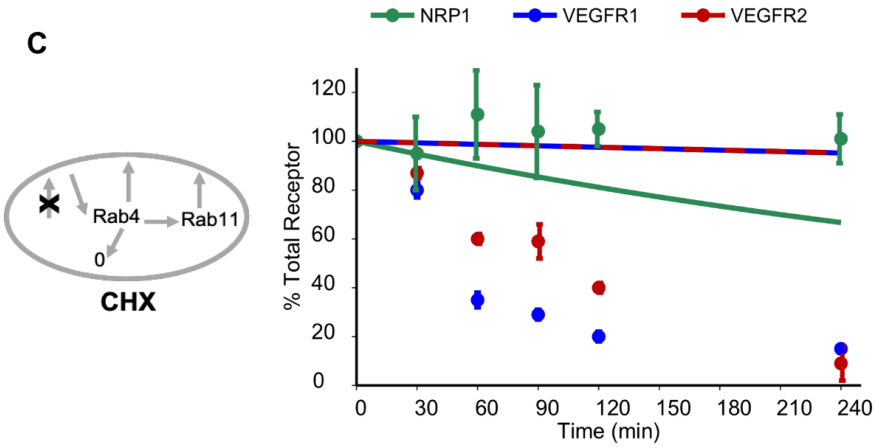

549

550 **Figure 3. Previous estimates of VEGFR trafficking parameters are not consistent with**
551 **HUVEC observations. A,** VEGFR2 and NRP1 trafficking parameters as previously estimated
552 using a computational model and published experimental data from porcine aortic endothelial
553 cells overexpressing human VEGFR2 and NRP1 [16]; and VEGFR1 parameters as then assumed

554 based on VEGFR2 parameters for computational models incorporating all three receptors [25].
555 **B,** Model-predicted levels ("Sim") of VEGFR1, VEGFR2 and NRP1 at steady state on the cell
556 surface and in intracellular endosomes (Rab4a/5a and Rab11a) using the 2015-2017 trafficking
557 parameters based mainly on PAEC data. Experimental data comparisons ("Exp") for surface
558 receptor levels are for HUVECs from this study. **C,** Simulations (lines) and experimental data
559 (dots) for whole-cell VEGFR1, VEGFR2, and NRP1 over time following CHX treatment. The
560 schematic shows how CHX inhibition of protein synthesis is represented in the model.
561

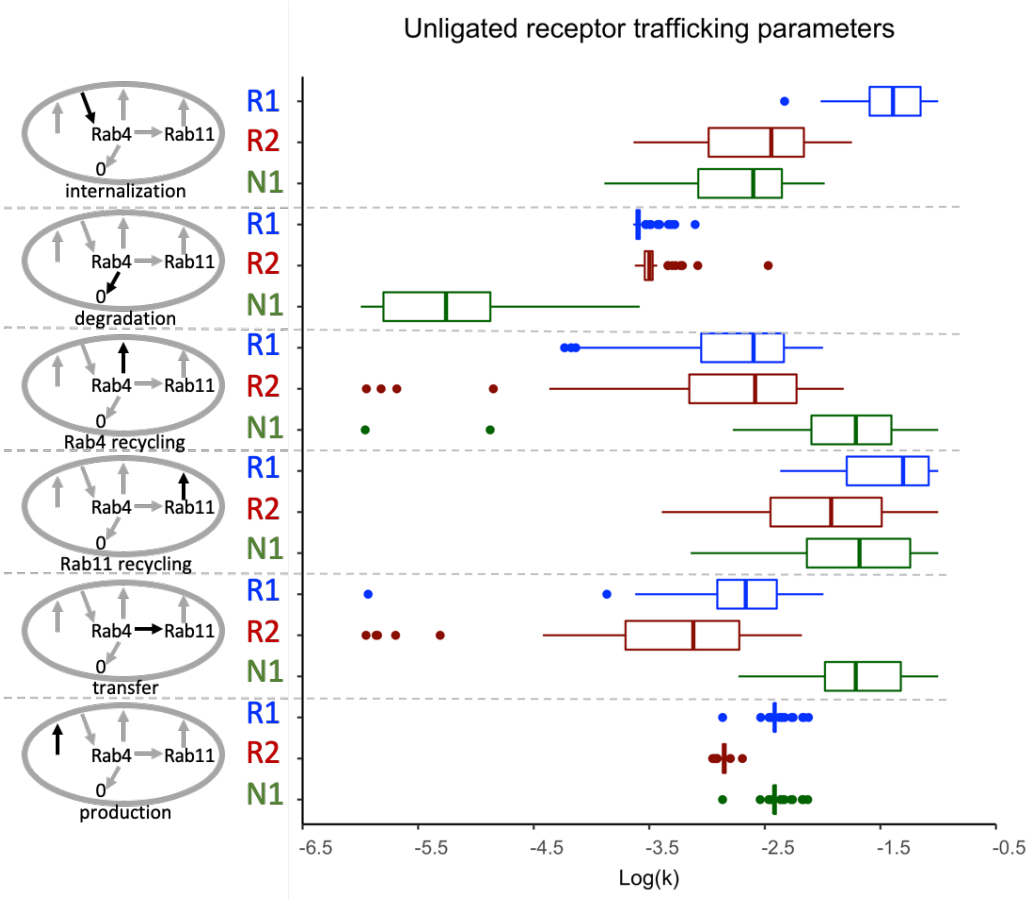

Figure 4. Trafficking parameter estimates for VEGFR1, VEGFR2, and NRP1 based on optimization to experimental data from HUVEC. While there is not one single unique optimization solution, the optimized parameter sets are well constrained, for most the majority of estimates are constrained within an order of magnitude. For each parameter, we used the median of the 76 optimizations to create a standard parameter set for use through the rest of the manuscript (see Supplementary Table S4 and Figure 5A).

570

A

Updated trafficking parameters (2022)				
Parameter	Description	VEGFR1 (s^{-1})	VEGFR2 (s^{-1})	NRP1 (s^{-1})
kint	Internalization	4.1×10^{-2}	3.6×10^{-3}	2.5×10^{-3}
kdeg	Degradation	2.5×10^{-4}	3.2×10^{-4}	5.5×10^{-6}
krec4	Early recycling	2.5×10^{-3}	2.6×10^{-3}	1.9×10^{-2}
k4to11	Pre-recycling	2.2×10^{-3}	7.6×10^{-4}	1.9×10^{-2}
krec11	Late recycling	5.0×10^{-2}	1.2×10^{-2}	2.1×10^{-2}
kprod	production rate	3.8×10^{-3}	1.5×10^{-3}	3.7×10^{-3}

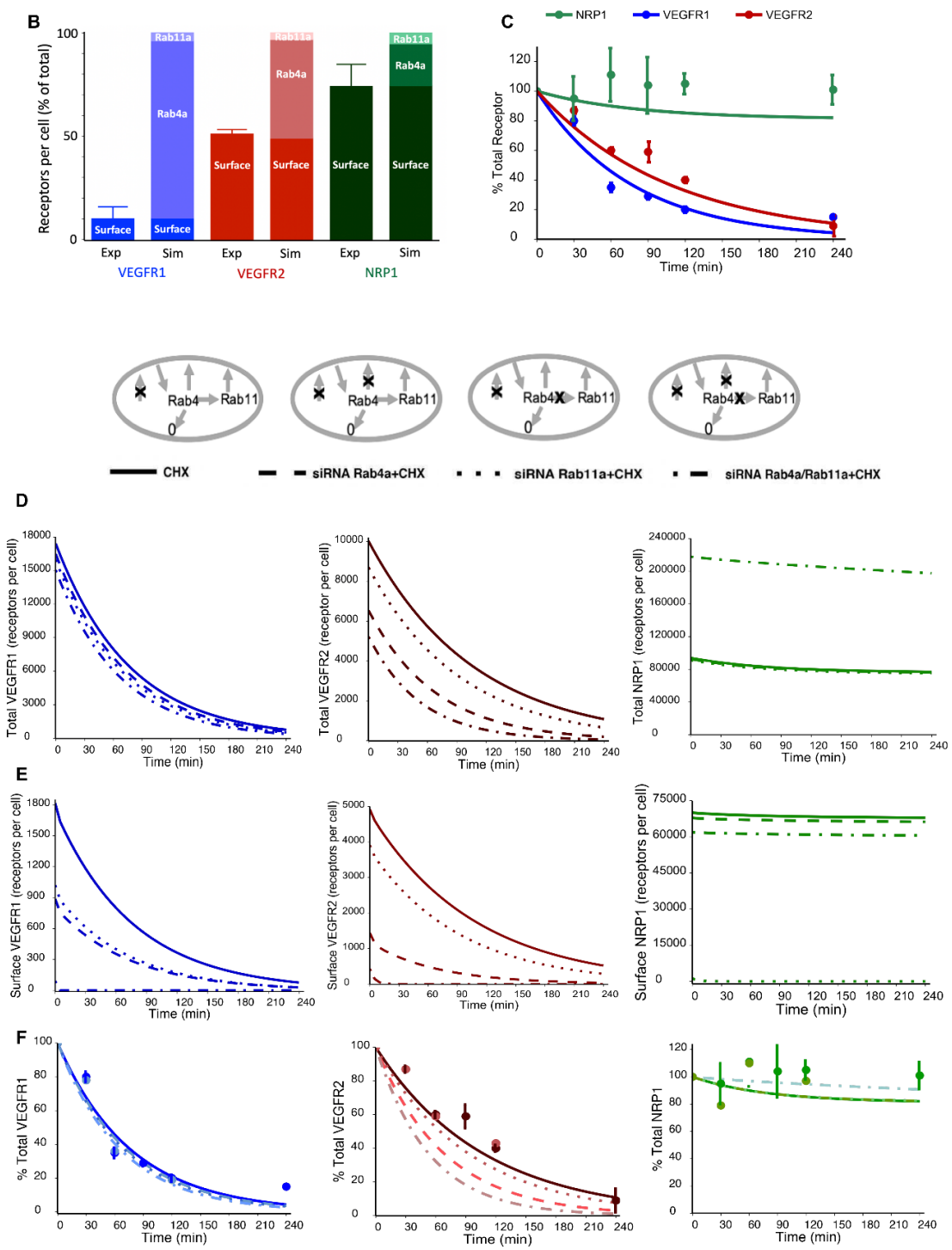

571
572 **Figure 5. Computational model predictions and model validation with trafficking**
573 **parameters. A,** Updated trafficking parameters for VEGFR1, VEGFR2, and NRP1 based on
574 geometric means of optimized parameter distributions. **B,** Surface, Rab4a/5a and Rab11a
575 distributions of unligated VEGFR1, VEGFR2 and NRP1 at steady state with the 2022 trafficking
576 parameters. Simulations ("Sim") and experimental data ("Exp") of surface VEGFR1, VEGFR2 and
577 NRP1 levels. **C,** Simulations (lines) and experimental data (dots) for whole-cell VEGFR1,
578 VEGFR2, and NRP1 over time following CHX treatment. **D-F,** Each panel shows the response to
579 CHX at time zero following no knockdown, Rab4a knockdown, Rab11a knockdown, and double
580 knockdown, for total (whole cell) (D, F) and surface (E) VEGFR1, VEGFR2, and NRP1. The
581 schematics show how the Rab knockdown experiments are represented in the model**.**
582
583

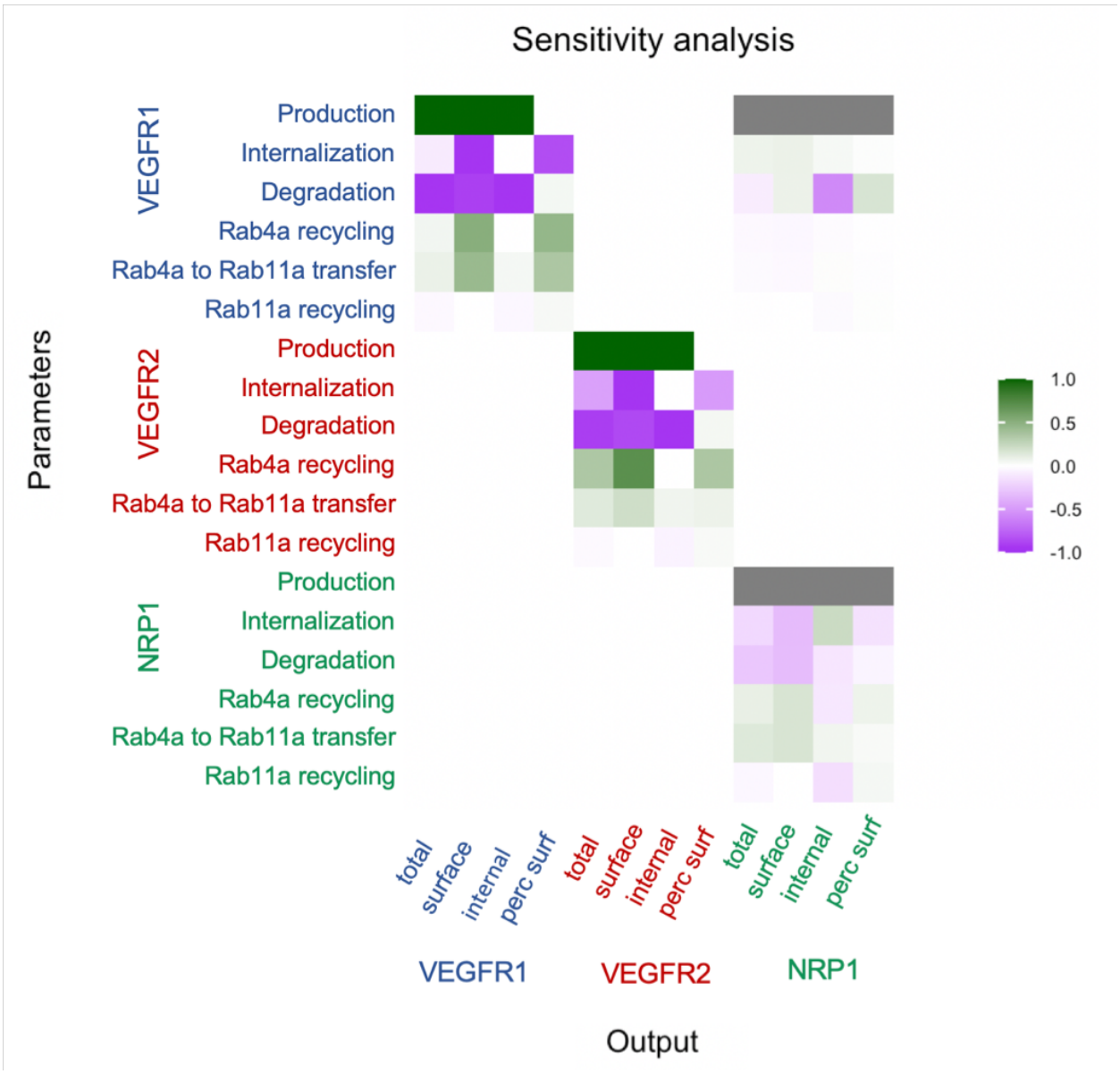

Figure 6. Sensitivity of model outputs to VEGFR1, VEGFR2 and NRP1 trafficking parameters. Local sensitivity analysis was performed by examining the sensitivity of model outputs to small changes in each of the 15 receptor trafficking and 3 receptor production parameters. Sensitivity values are the ratio of percent change in key model outputs (x-axis) to percent change in the parameter values (y-axis). The gray values represent higher than linear sensitivity that negatively (production of VEGFR1) or positively (production of NRP1) affect NRP1 levels due to the nonlinearity of VEGFR1-NRP1 interactions.

A

receptors/cell	VEGFR1	VEGFR2	NRP1
surface	1,800	4,900	68,000
internal	16,200	4,010	19,180
total	18,000	8,910	87,180

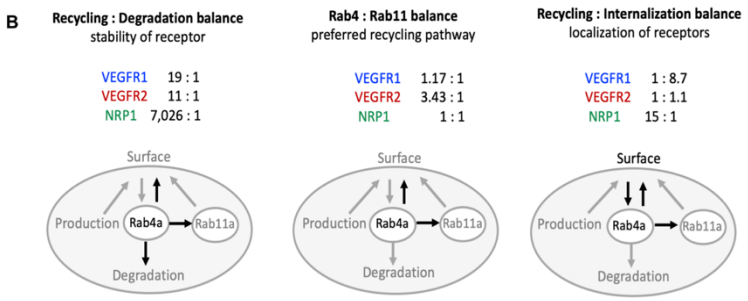

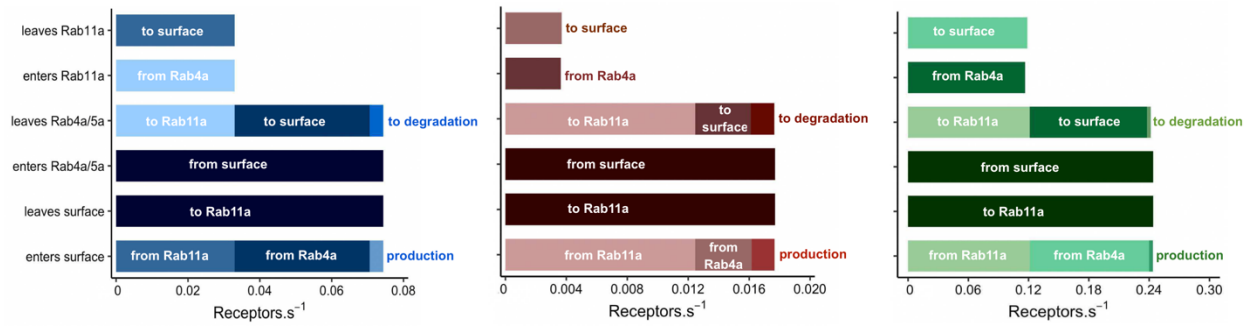

Figure 7. Transport rate analysis on differential transport of VEGFR1, VEGFR2 and NRP1. A, Receptor expression levels on the cell surface and intracellularly in our model without perturbation. The surface levels are as previously measured experimentally [26] and the internal levels are calculated here based on the surface levels and the percentage of each receptor on the surface based on the biotin labeling experiments (Figure 2). **B,** Mechanistic insights from trafficking parameters, informed by key ratios of rate constants. **C,** The overall transport rates (rate constant multiplied by concentration) for VEGFR1, VEGFR2 and NRP1 in each subcellular location. A rate constant could be high, but if the corresponding concentration is low (and the receptors are not uniformly distributed across cellular compartments), then the rate of movement will be low. At steady state, these overall rates in and out are balanced, so the 'net' rates are close to zero. For Rab11a: receptors arrive from Rab4a balances out by recycling, for Rab4a: receptors are internalized to Rab4a balances out the sum of degraded, recycling, and to Rab4a, for surface: receptor internalization balances the sum of new synthesis and recycling from Rab4a and Rab11a.

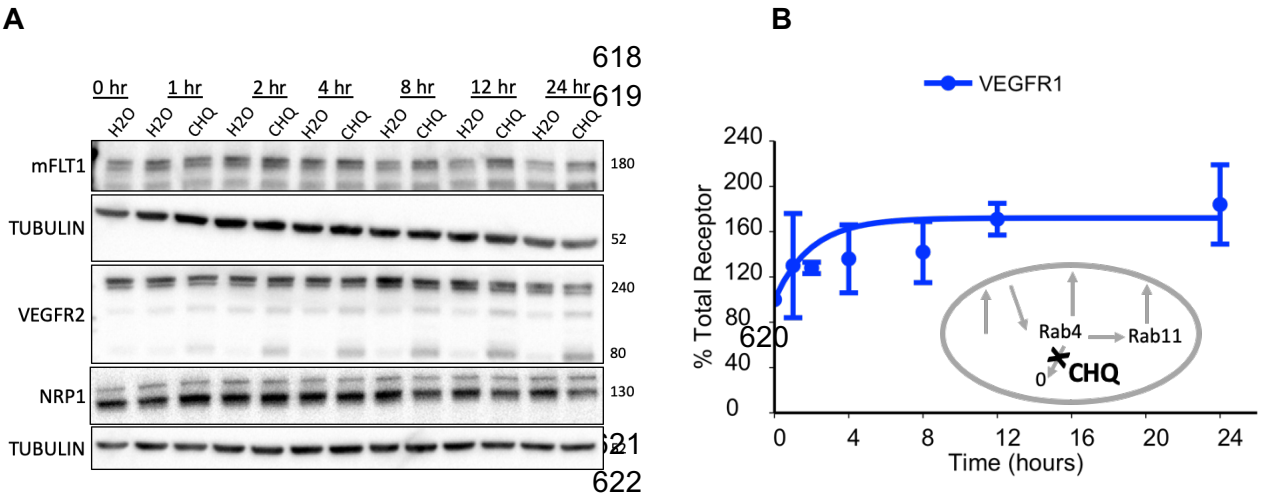

Figure 8. Impact of inhibiting lysosomal degradation on whole cell and surface VEGFR1, VEGFR2, NRP1 trafficking. Chloroquine (CHQ) treatment inhibits lysosomal degradation. **A,** Western blot of total (whole cell) VEGFR1, VEGFR2, NRP1 levels after indicated times of CHQ treatment. **B,** Comparison of simulation result (line) and quantification of Western blot (dot) for whole cell VEGFR1 levels after indicated times of CHQ treatment.

632 **References**

633 1. Annex BH. Therapeutic angiogenesis for critical limb ischaemia. Nat Rev Cardiol. 2013;10:
634 387–396.
635 2. Annex BH, Cooke JP. New directions in therapeutic angiogenesis and arteriogenesis in
636 peripheral arterial disease. Circ Res. 2021;128: 1944–1957.
637 3. Mac Gabhann F, Annex BH, Popel AS. Gene therapy from the perspective of systems
638 biology. Curr Opin Mol Ther. 2010;12: 570.
639 4. Simons M, Gordon E, Claesson-Welsh L. Mechanisms and regulation of endothelial VEGF
640 receptor signalling. Nat Rev Mol Cell Biol. 2016;17: 611–625.
641 doi:https://doi.org/10.1038/nrm.2016.87
642 5. Sarabipour S, Ballmer-Hofer K, Hristova K. VEGFR-2 conformational switch in response to
643 ligand binding. eLife. 2016;5: e13876. doi:http://doi.org/10.7554/eLife.13876
644 6. da Rocha-Azevedo B, Lee S, Dasgupta A, Vega AR, de Oliveira LR, Kim T, et al.
645 Heterogeneity in VEGF Receptor-2 Mobility and Organization on the Endothelial Cell
646 Surface Leads to Diverse Models of Activation by VEGF. Cell Rep. 2020;32: 108187.
647 7. Chappell JC, Bautch VL. Vascular development: genetic mechanisms and links to vascular
648 disease. Curr Top Dev Biol. 2010;90: 43–72.
649 8. Markovic-Mueller S, Stuttfeld E, Asthana M, Weinert T, Bliven S, Goldie KN, et al. Structure
650 of the Full-length VEGFR-1 Extracellular Domain in Complex with VEGF-A. Structure.
651 2017;25: 341–352. doi:https://doi.org/10.1016/j.str.2016.12.012
652 9. Bautch VL. VEGF-directed blood vessel patterning: from cells to organism. Cold Spring
653 Harb Perspect Med. 2012;2: a006452.
654 10. Kendall R, Thomas K. Inhibition of vascular endothelial cell growth factor activity by an
655 endogenously encoded soluble receptor. Proc Natl Acad Sci U S A. 1993;90: 10705–1070.
656 doi:https://doi.org/10.1073/pnas.90.22.10705
657 11. Ganta VC, Choi M, Kutateladze A, Annex BH. VEGF165b Modulates Endothelial VEGFR1–
658 STAT3 Signaling Pathway and Angiogenesis in Human and Experimental Peripheral Arterial
659 Disease. Circ Res. 2016;120: 282–295.
660 doi:https://doi.org/10.1161/CIRCRESAHA.116.309516
661 12. Ganta VC, Choi M, Farber CR, Annex BH. Antiangiogenic VEGF165b Regulates
662 Macrophage Polarization via S100A8/S100A9 in Peripheral Artery Disease. Circulation.
663 2018;139: 226–242. doi:https://doi.org/10.1161/CIRCULATIONAHA.118.034165
664 13. Nesmith JE, Chappell JC, Cluceru JG, Bautch VL. Blood vessel anastomosis is spatially
665 regulated by Flt1 during angiogenesis. Development. 2017;144: 889–896.
666 doi:http://doi.org/10.1242/dev.145672
667 14. Karaman S, Paavonsalo S, Heinolainen K, Lackman MH, Ranta A, Hemanthakumar KA, et
668 al. Interplay of vascular endothelial growth factor receptors in organ-specific vessel
669 maintenance. J Exp Med. 2022;219: e20210565.
670 15. Sadowski L, Pilecka I, Miaczynska M. Signaling from endosomes: Location makes a
671 difference. Exp Cell Res. 2009;315: 1601–1609.
672 doi:https://doi.org/10.1016/j.yexcr.2008.09.021
673 16. Wendel Clegg L, Mac Gabhann F. Site-Specific Phosphorylation of VEGFR2 Is Mediated by
674 Receptor Trafficking: Insights from a Computational Model. PLOS Comput Biol. 2015;11:
675 e1004158. doi:https://doi.org/10.1371/journal.pcbi.1004158
676 17. Smith GA, Fearnley GW, Tomlinson DC, Harrison MA, Ponnambalam S. The cellular
677 response to vascular endothelial growth factors requires co-ordinated signal transduction,
678 trafficking and proteolysis. Biosci Rep. 2015;35: e00253.
679 18. Boucher JM, Clark RP, Chong DC, Citrin KM, Wylie LA, Bautch VL. Dynamic alterations in
680 decoy VEGF receptor-1 stability regulate angiogenesis. Nat Commun. 2017;8: 15699.
681 doi:https://doi.org/10.1038/ncomms15699

682 19. Jopling HM, Howell GJ, Gamper N, Ponnambalam S. The VEGFR2 receptor tyrosine kinase
683 undergoes constitutive endosome-to-plasma membrane recycling. Biochem Biophys Res
684 Commun. 2011;410: 170–176.
685 20. Gampel A, Moss L, Jones MC, Brunton V, Norman JC, Mellor H. VEGF regulates the
686 mobilization of VEGFR2/KDR from an intracellular endothelial storage compartment. Blood.
687 2006;108: 2624–2631. doi:https://doi.org/10.1182/blood-2005-12-007484
688 21. Bruns AF, Herbert SP, Odell AF, Jopling HM, Hooper NM, Zachary IC, et al. Ligand-
689 stimulated VEGFR2 signaling is regulated by co-ordinated trafficking and proteolysis.
690 Traffic. 2010;11: 161–174.
691 22. Ballmer-Hofer K, Andersson AE, Ratcliffe LE, Berger P. Neuropilin-1 promotes VEGFR-2
692 trafficking through Rab11 vesicles thereby specifying signal output. Blood. 2011;118: 816–
693 826. doi:https://doi.org/10.1182/blood-2011-01-328773
694 23. Jopling HM, Odell AF, Pellet-Many C, Latham AM, Frankel P, Sivaprasadarao A, et al.
695 Endosome-to-plasma membrane recycling of VEGFR2 receptor tyrosine kinase regulates
696 endothelial function and blood vessel formation. Cells. 2014;3: 363–385.
697 24. Mac Gabhann F, Popel AS. Model of competitive binding of vascular endothelial growth
698 factor and placental growth factor to VEGF receptors on endothelial cells. Am J Physiol-
699 Heart Circ Physiol. 2004;286: H153–H164.
700 25. Wendel Clegg L, Mac Gabhann F. A computational analysis of in vivo VEGFR activation by
701 multiple co-expressed ligands. PLOS Comput Biol. 2017;13: e1005445.
702 doi:https://doi.org/10.1371/journal.pcbi.1005445
703 26. Imoukhuede PI, Popel AS. Quantification and cell-to-cell variation of vascular endothelial
704 growth factor receptors. Exp Cell Res. 2011;317: 955–965.
705 doi:https://doi.org/10.1016/j.yexcr.2010.12.014
706 27. Harris LA, Hogg JS, Tapia J-J, Sekar JAP, Gupta S, Korsunsky I, et al. BioNetGen 2.2:
707 advances in rule-based modeling. Bioinformatics. 2016;32: 3366–3368.
708 doi:https://doi.org/10.1093/bioinformatics/btw469
709 28. Calera MR, Venkatakrishnan A, Kazlauskas A. VE-cadherin increases the half-life of VEGF
710 receptor 2. Exp Cell Res. 2004;300: 248–56. doi:https://doi.org/10.1016/j.yexcr.2004.07.007
711 29. Mittar S, Ulyatt C, Howell GJ, Bruns AF, Zachary I, Walker JH, et al. VEGFR1 receptor
712 tyrosine kinase localization to the Golgi apparatus is calcium-dependent. Exp Cell Res.
713 2009;315: 877–889.
714 30. Napione L, Pavan S, Veglio A, Picco A, Boffetta G, Celani A, et al. Unraveling the influence
715 of endothelial cell density on VEGF-A signaling. Blood. 2012;119: 5599–5607.
716 doi:https://doi.org/10.1182/blood-2011-11-390666
717 31. Wu FTH, Stefanini MO, Mac Gabhann F, Popel AS. A Compartment Model of VEGF
718 Distribution in Humans in the Presence of Soluble VEGF Receptor-1 Acting as a Ligand
719 Trap. PLoS ONE. 2009;4: e5108. doi:https://doi.org/10.1371/journal.pone.0005108
720 32. Fuh G, Garcia KC, de Vos AM. The interaction of neuropilin-1 with vascular endothelial
721 growth factor and its receptor flt-1. J Biol Chem. 2000;275: 26690–26695.
722 33. Baumdick M, Brüggemann Y, Schmick M, Xouri G, Sabet O, Davis L, Chin JW, Bastiaens
723 PIH. EGF-dependent re-routing of vesicular recycling switches spontaneous
724 phosphorylation suppression to EGFR signaling. eLife. 2015;4: e12223.
725 https://doi.org/10.7554/eLife.12223